Climate Dynamics (2024) 62:2907–2924
https://doi.org/10.1007/s00382-024-07210-5

Near-global summer circulation response to the spring surface temperature anomaly in Tibetan Plateau –– the GEWEX/LS4P first phase experiment

Yang Zhang[1] · Yan Pan[1,2] · Yongkang Xue[3] · Ismaila Diallo[4] · Xubin Zeng[5] · Shuting Li[1] · J. David Neelin[3] · William K. M. Lau[6] · Aaron A. Boone[7] · Frederic Vitart[8] · Tandong Yao[9] · Qi Tang[10] · Tomonori Sato[11] · Myung-Seo Koo[12] · Constantin Ardilouze[7] · Subodh K. Saha[13] · Jing Yang[14] · Stefano Materia[15] · Zhaohui Lin[16] · Xin Qi[14] · Yi Qin[17] · Tetsu Nakamura[11] · Paulo Nobre[18] · Daniele Peano[19] · Retish Senan[8] · Yuhei Takaya[20] · Hailan Wang[21] · Hongliang Zhang[22] · Yanling Zhan[16] · Mei Zhao[23] · Carlos R. Mechoso[3] · Qing Bao[24] · Marcus Jorge Bottino[18] · Songyou Hong[11,25] · Yanluan Lin[26] · Shaocheng Xie[10] · Xiaoduo Pan[9] · Hara Prasad Nayak[3] · Sin Chan Chou[18] · Weidong Guo[1]

Received: 31 July 2023 / Accepted: 19 March 2024 / Published online: 29 March 2024
© The Author(s) 2024, corrected publication 2024

Abstract
Subseasonal to seasonal (S2S) prediction of droughts and floods is one of the major challenges of weather and climate prediction. Recent studies suggest that the springtime land surface temperature/subsurface temperature (LST/SUBT) over the Tibetan Plateau (TP) can be a new source of S2S predictability. The project "Impact of Initialized Land Surface Temperature and Snowpack on Subseasonal to Seasonal Prediction (LS4P)" was initiated to study the impact of springtime LST/SUBT anomalies over high mountain areas on summertime precipitation predictions. The present work explores the simulated global scale response of the atmospheric circulation to the springtime TP land surface cooling by 16 current state-of-the-art Earth System Models (ESMs) participating in the LS4P Phase I (LS4P-I) experiment. The LS4P-I results show, for the first time, that springtime TP surface anomalies can modulate a persistent quasi-barotropic Tibetan Plateau-Rocky Mountain Circumglobal (TRC) wave train from the TP via the northeast Asia and Bering Strait to the western part of the North America, along with the springtime westerly jet from TP across the whole North Pacific basin. The TRC wave train modulated by the TP thermal anomaly play a critical role on the early summer surface air temperature and precipitation anomalies in the regions along the wave train, especially over the northwest North America and the southern Great Plains. The participant models that fail in capturing the TRC wave train greatly under-predict climate anomalies in reference to observations and the successful models. These results suggest that the TP LST/SUBT anomaly via the TRC wave train is the first order source of the S2S variability in the regions mentioned. Furthermore, the TP surface temperature anomaly can influence the Southern Hemispheric circulation by generating cross-equator wave trains. However, the simulated propagation pathways from the TP into the Southern Hemisphere show large inter-model differences. More dynamical understanding of the TRC wave train as well as its cross-equator propagation into the Southern Hemisphere will be explored in the newly launched LS4P phase II experiment.

1 Introduction

The successful prediction of droughts and floods at subseasonal-to-seasonal (S2S) time scales is one of the major challenges of weather and climate prediction, with failures that can result in major adverse impacts on societies and economies (Vitart 2017; Robertson et al. 2018; Merryfield et al. 2020). Improving the prediction skill at S2S timescale requires a further understanding of the mechanisms at work for climate variabilities at this timescale as well as the identification of predictability sources. Sea surface temperature (SST) variations such as those associated with the Madden-Julian Oscillations (e.g., Vitart 2017; Woolnough 2019) are known to provide a predictability source. Recent studies suggest that springtime land surface/subsurface temperature (LST/SUBT) provides a new source of predictability at S2S time scales (Xue et al. 2016, 2018). The Global Energy

Extended author information available on the last page of the article

and Water Exchanges (GEWEX) program has initiated the project "Impact of Initialized Land Surface Temperature and Snowpack on Subseasonal to Seasonal Prediction (LS4P)" to investigate the impact of springtime LST/SUBT anomalies over high mountain areas on summertime precipitation predictions (Xue et al. 2021).

The first phase of the LS4P project (LS4P-I), in which more than 40 institutions worldwide have participated, has focused on the effect of spring LST/SUBT in the Tibetan Plateau (TP) on the S2S precipitation predictions for the following summer. Using an innovative initialization method for land surface/subsurface temperatures over TP (Xue et al. 2021), simulations by Earth System Models (ESMs) participating in LS4P-I have shown that TP springtime LST/SUBT anomalies can affect summer precipitation not only in the East Asia but also over many regions in the world through teleconnections. Analysis of observations and simulation results identified 8 hot spot regions in the world where June precipitation anomalies are significantly correlated with the anomalies in TP May 2 m surface air temperature (T2m). Most of the hot spot regions are heavily populated and host major economic activity. For these regions, the TP LST/SUBT anomaly is the first order source of the S2S variability, comparable with the influence of SST. Among these connections, a strong linkage between the spring TP LST/SUBT and the summer precipitation over the west of North America was found, and a Tibetan Plateau-Rocky Mountain Circumglobal (TRC) wave train from the TP through northeast Asia and Bering Strait to the west of North America had been identified for the first time based on the reanalysis data and suggested to be responsible for the formation of most of the hotspots (Xue et al. 2022, 2023). Although the teleconnections caused by the heating due to oceanic temperature anomalies, such as those between ENSO and the Asian monsoons, have been extensively investigated (e.g., Wang et al. 2000; Li et al. 2007; Li et al. 2017), the remote effects of mountain heating on global atmospheric circulations have not been fully studied. The LS4P-I experiment provides a chance to explore the detailed features of the TRC wave train as well as the global response of atmospheric circulations to the TP surface anomaly.

The present study is a follow-up of Xue et al. (2023), which analyzed the results of LS4P-I and explored mechanisms through which TP LST/SUBT affects the East Asian summer monsoon. Our aim is to place the TP LST/SUBT's influence on the global atmospheric circulations with a focus on the dynamical feature of the TRC wave train and its importance for improving S2S prediction. The analysis to be presented shows that, on the background of springtime westerly jet across the North Pacific basin, the persistent TP surface cold anomaly can generate a quasi-barotropic, slowly evolving wave train extending from the TP to the northwest of North America in May and June, through which TP surface anomaly can act as a first order source of the S2S variability for these regions. Furthermore, the wave train can also extend southward along the west coast of America reaching the northern Southern Hemisphere and result in the global atmospheric circulation response to the cold TP surface.

The manuscript is organized as follows. Section 2 introduces the design of the LS4P Phase I experiment and compares the model ensemble with observations. Section 3 analyzes the model ensemble of the global response of the atmospheric circulation to the cold TP LST/SUBT anomaly, with the focus on the feature of TRC wave train. Section 4 explores the relationship between the TRC wave train and the T2m, precipitation anomalies. Section 5 discusses the Southern Hemispheric extension of the wave train. Summary and discussions are provided in Section 6.

2 LS4P first phase experiments

The detailed experiment designs and basic results of the LS4P first phase experiments have been documented in Xue et al. (2021) and Xue et al. (2022, 2023), respectively. In this section, we briefly introduce the basic information. In the first phase of the LS4P project (LS4P-I), the year 2003 is the focal case, in which extreme summer drought/flood occurred in East Asia after a very cold spring in the TP. Two sets of numerical experiments were conducted in LS4P-I to investigate the global influence of the TP spring surface temperature anomaly (all seasons refer to the Northern Hemisphere in the following, and hereafter the exact range of TP refers to the region where the elevation is over 4000 m). Details of the 16 state-of-the-art earth system models (ESMs) participating in LS4P-I are listed in Table S1 in the Supplementary Information. A first set of runs, referred to as EXP_CTRL, is designed to evaluate the performance of the 16 ESMs in simulating the TP T2m and precipitation anomalies during May and June 2003. In EXP_CTRL runs, the ESMs start simulations from late April or May 1st, and use the standard S2S prediction setting of atmospheric and land initial conditions. In most runs, the observed sea surface temperature (SST) and sea ice conditions are prescribed in the boundary conditions. However, the runs by the CNRM-CM6-I-CMIP and ECMWF-IFS are performed in a fully coupled atmosphere-land-ocean configuration, in which only the ocean initial condition is prescribed. Each ESMs conducted ensembles of at least six members for each run, with most groups providing ensembles of more than ten members as shown in Table S1. For each model, we select the output for the May 1st-June 30th period, interpolate it onto a regular $0.5° \times 0.5°$ global grid using the bilinear interpolation method, and calculate the ensemble-mean of the model output to reduce the influence of the atmospheric

internal variability on the experiment result. More details of the model configurations and experiment designs of the EXP_CTRL run are documented in Xue et al. (2021).

As shown in Xue et al. (2023), in EXP_CTRL run most LS4P-I ESMs produce reasonable global scale climate features, such as the large-scale monsoon circulations, strong June precipitations in the Intertropical Convergence Zone (ITCZ) and a second precipitation peak in midlatitudes. However, model biases are evident at the regional scale. The observed T2m anomaly in the TP is shown in Fig. 1a, for which we use the data from the National Oceanic and Atmospheric Administration (NOAA) Climate Anomaly Monitoring System (CAMS, Fan and van den Dool 2008). Compared with the observation, none of the LS4P-I ESMs well captures the observed T2m cold anomaly in May 2003. The ensemble mean of the 16 LS4P-I ESMs exhibits a warm bias of 1.02 °C over the TP (see Table S2 and the supplementary information in Xue et al. 2023 for details), which is stronger than the standard deviation of the observed inter-annual variation of TP T2m (about 0.7 °C). The spatial distribution of the model bias for the ensemble mean is shown in Fig. 1b, which shows a clear warm bias in May 2003 T2m over the eastern part of the TP. Note that the bias here is defined for the case of 2003, which is the difference between the multi-model ensemble mean and the corresponding observation. To have a comprehensive assessment for models' bias, more cases are necessary. Along with this model bias in the May T2m over TP, evident biases in June precipitation are also found not only in East Asia but also in many other regions such as the central U.S. and South America (shown in Xue et al. 2023).

Another set of numerical experiments was carried out by the ESMs to test whether the regional bias in June precipitation mentioned in the previous paragraph is related to the bias in May surface temperature over TP. In this set of experiments, which are collectively referred to as EXP_LST/SUBT run, the models' bias in May TP T2m is reduced by initializing the TP LST and SUBT conditions. A comparison between results in CTRL and LST/SUBT runs thus allows for an assessment of the extent to which the improved simulation of the May TP T2m anomaly impacts the June precipitation. Therefore, all initial and boundary conditions in EXP_LST/SUBT run are identical to those in the EXP_CTRL run, except that the LST and SUBT in each grid over TP region are initialized as in Xue et al. (2021). Since the LS4P-I models have both warm and cold biases over TP, for the ESMs with warm/cold bias, the initialization in the EXP_LST/SUBT run would make the initial LST and SUBT cooler/warmer than in the EXP_CTRL run, respectively. To investigate the remote effect of the cold May TP

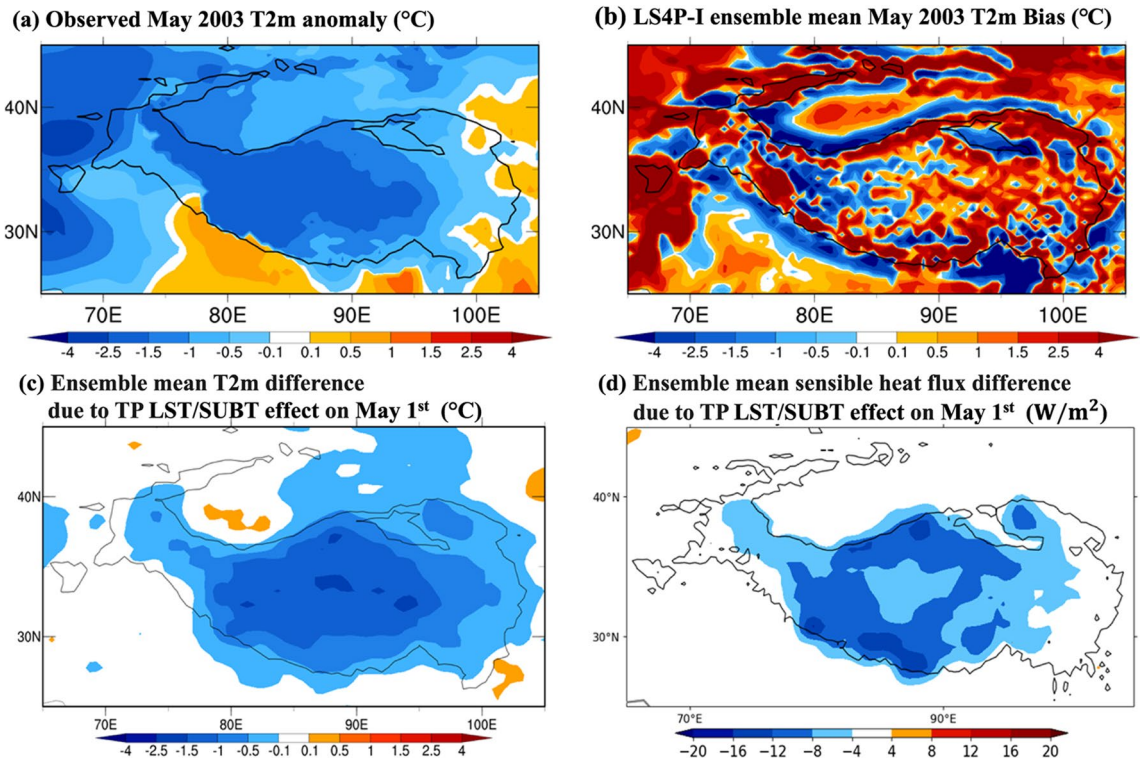


Fig. 1 **a** Observed May 2003 T2m anomaly (℃); **b** simulated ensemble mean May 2003 T2m bias (℃) in EXP_CTRL run; **c** simulated ensemble mean T2m differences and **d** simulated ensemble mean surface sensible heat flux differences on May 1st due to the TP LST/SUBT effect. The black contour outlines the region above 3000 m in this and following figures unless otherwise stated

surface anomaly, for each model's ensemble mean of the EXP_CTRL and EXP_LST/SUBT runs, we compose the simulation with cooler/warmer initial condition over the TP into the Cold case/Warm case, respectively, as in Xue et al. (2022). We refer to the simulated difference of the ensemble mean between Cold and Warm cases as to the TP LST/SUBT effect. The multi-model ensemble mean of the difference between Cold and Warm cases can further reduce the inter-model variation and indicates the influence of the cold TP LST/SUBT simulated by the 16 state-of-the-art models.

Figure 1c, d show the simulated ensemble mean of T2m and surface sensible heat flux differences due to the TP LST/SUBT effect on May 1st, which is around the beginning of the simulation. These differences approximately represent the impact of LST/SUBT initialization and associated surface thermal forcing exerted on the atmosphere. As shown in Fig. 1c, the LST/SUBT initialization results in TP cold surface anomalies that are more like the observed May T2m cold anomaly in 2003 (Fig. 1a) though with weaker magnitudes. Above the colder TP surface, the surface sensible heat flux is reduced. Such a surface cooling can last for more than a month, affecting the atmospheric circulations in regional and even global scales.

To investigate the extent to which the TP surface cooling can explain the observed anomalies in atmospheric circulations, surface air temperature and precipitation in the year 2003, the ensemble mean of the LS4P-I experiment is also compared with the observation. We use the fifth generation ECMWF atmospheric reanalysis (ERA5, Hersbach et al. 2020), which is referred to as observations, with a regular horizontal resolution of $1.0° \times 1.0°$ to investigate the atmospheric circulation in year 2003 and for climatology, with the latter defined as the average from year 1981 to 2015. All data are provided at $0.5° \times 0.5°$ spatial resolution. The global precipitation data are from the Climate Research Unit (CRU), in which version 4.02 is used when implementing the analysis (Harris et al. 2014; 2020).

Figure 2a shows the ensemble mean differences in May and June averaged 2 m air temperature due to the TP LST/SUBT effect alongside with the observed May-June T2m anomalies in year 2003 (Fig. 2b). The model results show that the LST/SUBT initialization over the TP produces persistent cold T2m anomalies in the region in May and June. Though the magnitude of the cold T2m anomaly decays from -1.0 °C since May 1st, the simulated two-month average exhibits a 73% of the observed TP averaged cooling (-0.80 °C) as in Fig. 2b. With the persistent surface cold anomaly over TP, Fig. 2a also exhibits evident and statistically significant T2m differences in many parts of the world. A comparison with the observed T2m anomalies (Fig. 2b) reveals that the model ensemble produces consistent temperature anomalies over northeast Asia, Bering Strait, Alaska, west coast of North America of the U.S. and even parts of South America. These features are generally in agreement with the path of TRC wave train, suggesting that the cold TP surface through the TRC wave train is one of the reasons for the observed spring temperature anomalies in the above regions. Particularly, a significant out of phase change of T2m with the TP is found around the Rocky Mountain, consistent with the finding from the observed inter-annual variation of T2m in the two regions in Xue et al. (2022). For other areas, such as West Europe and northern Siberia, the simulated differences are not consistent with observations. The reasons for the T2m anomalies in those regions and whether they are caused by external forcings other than the TP surface anomaly need to be further investigated.

The key features of the simulated ensemble mean of June precipitation in response to the TP LST/SUBT effect were discussed in Xue et al. (2022). A selection of these features in Fig. 3a shows that the TP LST/SUBT effect can lead to global scale precipitation anomalies. In particular, Fig. 3a highlights the eight hot spots identified in Xue et al. (2022), in which the TP LST/SUBT effect produces significant precipitation differences which have counterparts in the observed June precipitation anomaly (Fig. 3b). More precise geographical locations of the eight hot spots are given in Table S3 in the Supplementary Information. Among the eight hot spots, there are at least six downstream of the TP: (1) southern Yangtze River Basin, (2) northeast Asia, (3) northwest North America, (4) Southern Great Plains, (5) Central America, and (6) northern South America. These six hot spots greatly overlap with the regions in Fig. 2 where the imposed TP LST/SUBT initial condition produce T2m anomalies in May and June with the same sign as in the observations. These regions are all along the TRC wave train, suggesting its key role in establishing TP's global influence on S2S time scales. (The simulated ensemble mean of May precipitation in response to the TP LST/SUBT effect is also documented in Figure S1.)

3 Atmospheric response to Tibetan surface cooling and the TRC wave train

LS4P-I has identified the TRC wave train and conjectures that this is a key process affecting the S2S predictability using the TP LST/ SUBT anomaly (Xue et al. 2022, 2023). This paper presents a comprehensive discussion on the dynamical features of the TRC wave train at the global scale. The upper-level westerly jet provides a wave guide for planetary scale wave trains. We examine the atmospheric response to a cold TP surface from the ensemble mean simulation of the May upper level (200 hPa) zonal wind differences by the 16 ESMs (Fig. 4a). For comparison, the observed 200 hPa zonal wind anomalies for 2003 (i.e., differences between such year and the climatology) are plotted in Fig. 4b. In

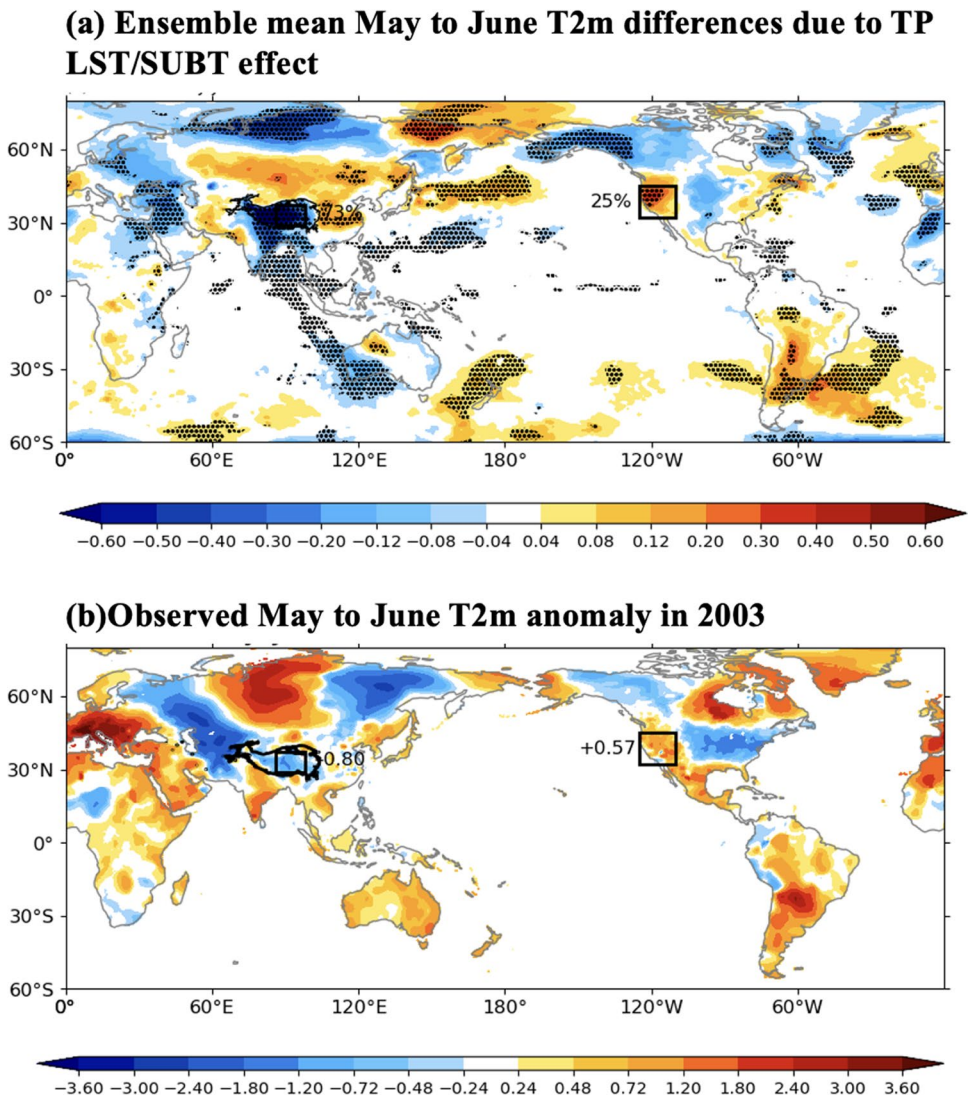


Fig. 2 May and June averaged 2 m air temperature (°C) differences **a** due to the TP LST/SUBT effect, and **b** between year 2003 and climatology (1981–2015 average) from CAMS reanalysis data. Note the different color bars used in panels (**a**) and (**b**). Black boxes outline the main region of TP (29N-37N, 86-98E) and Rocky Mountain (32-45N, 110-125W) as defined in Xue et al. (2022), beside which the values of the box-averaged T2m anomaly in observations are listed in panel (**b**) and the simulated percentages of the box-averaged T2m anomaly compared with observations are listed in panel (**a**). In panel (**a**), values above the 90% confidence level by Student's t-test are denoted by black dots

spring, the TP is just on the pathway of the upper-level westerly at mid-latitudes and the upstream of the East Asian Jet Core, which extends from east Asia through the North Pacific basin to the west coast of the North America and features the strongest wind speeds in the Northern Hemisphere.

The ensembles of ESM simulation capture this feature. The most evident response of the zonal wind occurs around the TP. The zonal wind becomes stronger to the south and weaker around the north edge of the TP. Such change is consistent with the thermal wind relationship, as the cold temperature over TP enhances the meridional temperature gradient to the south of the TP but weakens the one to the north. Furthermore, as demonstrated in previous studies (Nie et al. 2016; Jiang et al. 2017; Chan et al. 2020), the changes in background temperature gradient at midlatitudes also affect the activity of baroclinic eddies (Xue et al., 2023), which can further reinforce the zonal wind changes and further influence the zonal wind downstream as the eddies move downstream and interact with the zonal flow. The response of the zonal wind in the downstream of TP is consistent with these studies, exhibiting a significant deceleration of the zonal wind along the jet core over the North Pacific. Meanwhile, a significant acceleration of the zonal wind is found to the north of the jet core, indicating a slight northward shift of the jet stream. Such changes in the zonal wind have their counterparts in the observations (see Fig. 4b).

The ensemble mean of simulated 200 hPa geopotential height difference is also illustrated in Fig. 5a together with the observations for May 2003 (Fig. 5b), to further explore the atmospheric circulation responses to the TP LST/SUBT effect. One salient feature in Fig. 5a is the strong negative geopotential height anomaly over the TP at 200 hPa, accompanied with a cyclonic anomalous circulation. Such a circulation response corresponds to the cold anomaly over the TP, where the atmosphere sinks and induces negative potential height anomalies at upper levels. To the north of the TP's

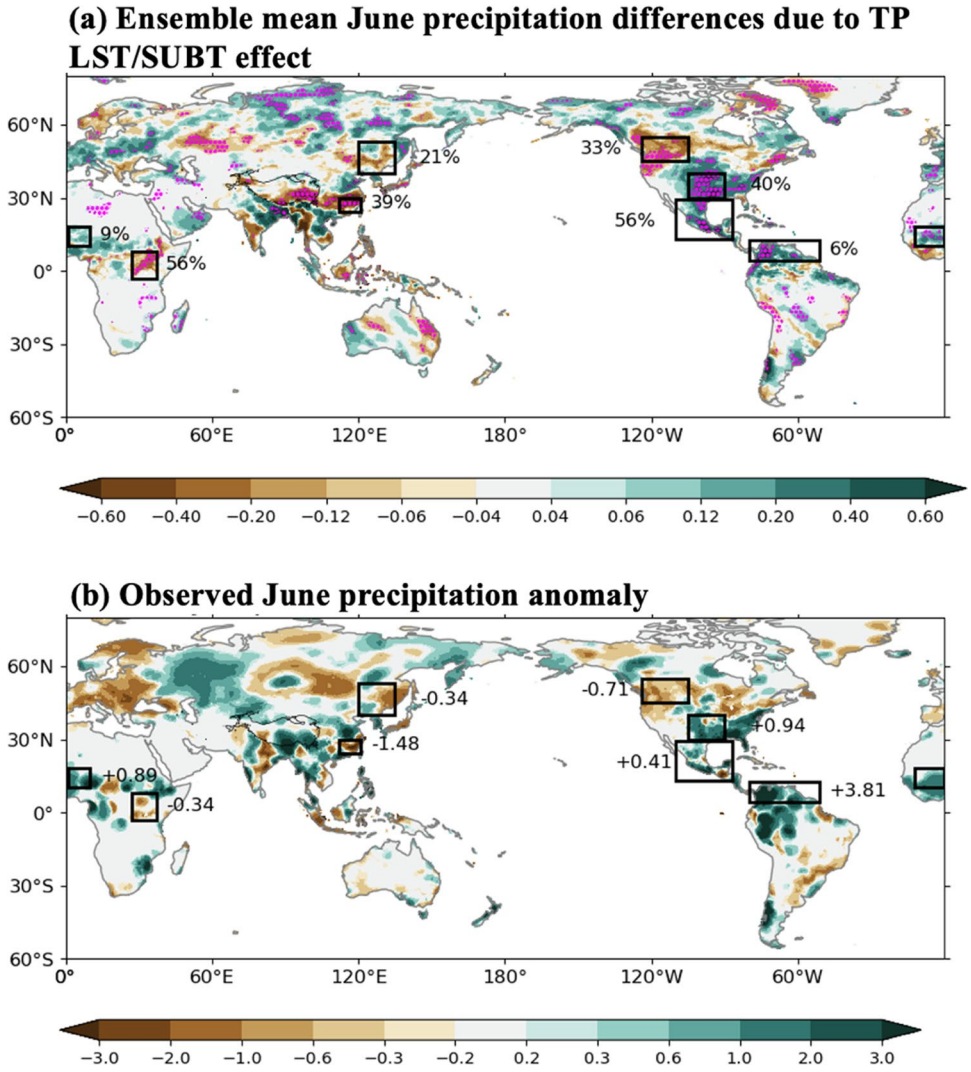


Fig. 3 June precipitation (mm/day) differences **a** due to the TP LST/SUBT effect, and **b** between year 2003 and climatology (1981–2015 average) from CRU data. Black boxes indicate regions where models produce consistent precipitation anomalies with the observation as in Xue et al. (2022), beside which the values of the box-averaged precipitation anomaly in observations are listed in panel (**b**) and the simulated percentages of the box-averaged precipitation anomaly compared with observations are listed in panel (**a**). Note the different colorbars used in panels (**a**) and (**b**). In panel (**a**), values above the 90% confidence level by Student's t-test are denoted by magenta dots

cold and cyclonic circulation center, clear positive geopotential height anomalies centered at 55°N with anti-cyclonic flow are found, forming a meridional dipole pair with the negative geopotential height center over TP, consistent with the observation in Fig. 5b.

Furthermore, evident wave like patterns downstream from the TP to the North Pacific are shown in the geopotential height difference in Fig. 5a. The negative center of geopotential height anomaly over the TP extends eastward to Japan, while a strong positive geopotential height center with anti-cyclonic circulation flow emerges to the east over the Bering Strait with a center around 170°E, 50°N. Downstream of this center, the figure shows a weaker negative geopotential height anomaly over the east North Pacific and a positive geopotential height anomaly around the Rocky Mountain in the west coast of North America. The wave like geopotential height differences further extend from the Rocky Mountain across the North American continent, North Atlantic Ocean and back to the Eurasian continent. The geopotential height differences in these action centers are all statically significant by Student's t-test. Most of the LS4P-1 models (at least 12 out of the 16 models) show consistent sign of geopotential height differences in these action centers as well (results not shown). As the geopotential height differences between the two groups of experiments are merely caused by the colder TP land surface in spring by initializing the TP LST and SUBT conditions, the above results show that the springtime cold TP surface can generate circumglobal changes in atmospheric circulation.

The above simulated response in atmospheric circulations is in general consistent with the observed geopotential height anomalies in May 2003 (Fig. 5b). The wave like pattern in geopotential height anomalies are also observed from TP through Bering Strait to the Rocky Mountain as well as the east coast of North America, though with slight differences in locations of each action centers. However, over the regions from the North Atlantic to the Ural Mountains, the observed geopotential height anomalies show opposite signs

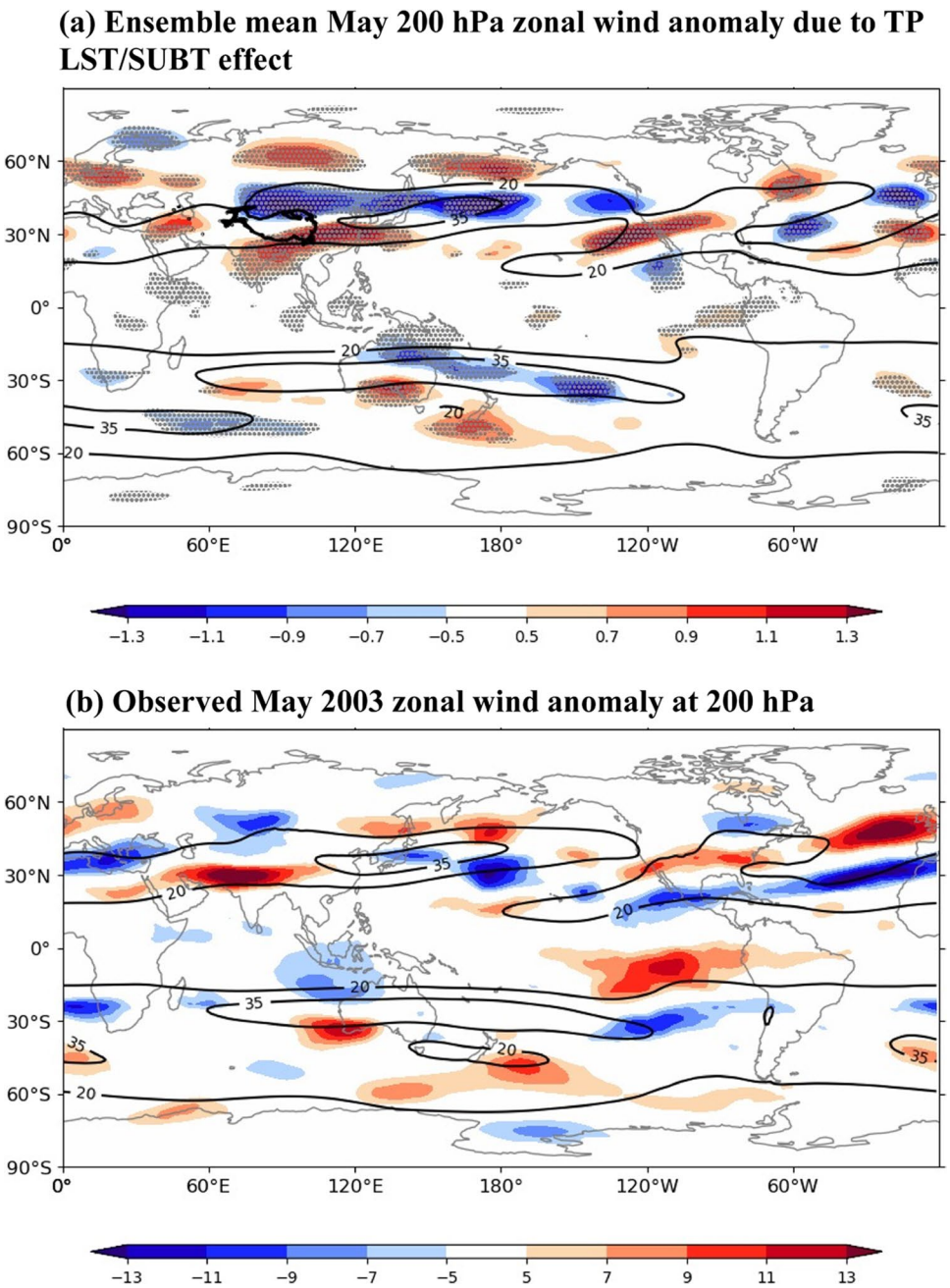


Fig. 4 Ensemble mean of the 200 hPa zonal wind differences (unit: m/s) in May **a** due to the TP LST/SUBT effect, and **b** between year 2003 and the climatology (1981–2015 average) from ERA5 reanalysis data. Black contours denote the zonal wind speed in EXP_CTRL run in panel (**a**) and the climatology in panel (**b**), respectively. In panel (**a**), gray dots denote values above the 90% confidence level by Student's t-test

to the multi-model average, suggesting that in those regions the TP surface cooling may not be the major cause for the observed circulation anomalies.

In addition, responses in the geopotential height to the cold TP surface are also noticed in the Southern Hemisphere, especially in the midlatitudes (Fig. 5a, b). The wave train like patterns with negative-positive-negative zonal structures extend along the whole Southern Ocean. However, there are phase differences between the simulated wave train and the observations. Similar and statistically significant patterns of the geopotential height anomaly are found around the Australia, South Pacific and South America. The anomaly amplitudes weaken in the tropics as the geostrophic approximation breaks down and connections become blurred. Therefore, we also inspect the anomalous stream function from the simulated wind.

To gain further insight into the dynamics of the TRC wave train, we also investigate the eddy stream function similar to Li et al. (2019) and the wave activity flux (WAF) following Takaya and Nakamura (2001). As shown in Li et al. (2019), the eddy stream function can better illustrate the wave train in both equatorial and extratropical regions. The WAF is parallel to the group velocity of Rossby waves and can approximately indicate the wave energy propagation

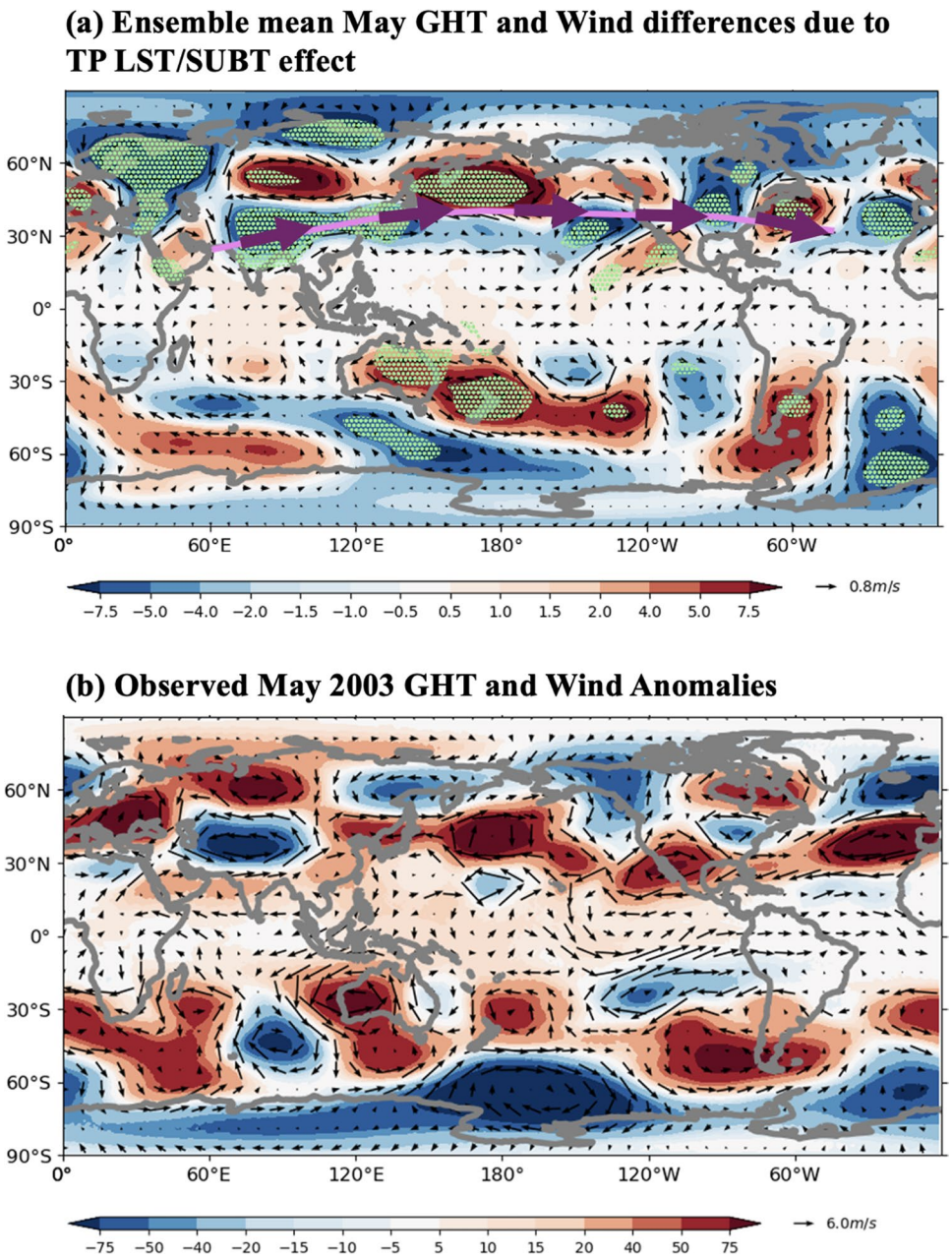


Fig. 5 Ensemble mean of 200 hPa geopotential height (shading, unit: m) and horizontal wind (vector, unit: m/s) differences in May (**a**) due to the TP LST/SUBT effect, and the observed May 200 hPa geopotential height differences between year 2003 and the climatology (average from 1981 to 2015) from ERA5 reanalysis data. In panel (**a**), the purple line with arrows suggests a possible pathway of wave train, and green dots indicate regions where values above the 90% confidence level by Student's t-test

(Takaya and Nakamura 2001; Gillett et al. 2022). Figure 6a shows the multi-model ensemble mean of the May WAF computed from the 200 hPa anomalous eddy stream function corresponding to the wind differences at 200 hPa due to the TP LST/SUBT effect. The most salient feature in Fig. 6a is the wave energy propagating through all the action centers from the TP, through northeast Asia, Bering Strait, Alaska to the Rocky Mountain region. After reaching the Rocky Mountain, the WAF further extends downstream across the North America, North Atlantic and back to the Eurasian continent, forming a "circumglobal" wave train. Furthermore, after the WAF reaching the Rocky Mountain from TP, there is another relatively small branch of wave train propagating southward along the west coast of America, even reaching the southern hemispheric midlatitudes, consistent with the responses in geopotential height, surface air temperature and June precipitation in South America. In addition, there are also weak signals emerging in the southern hemispheric low latitudes such as near the Indonesia and central Pacific with WAF propagating to the mid-latitudes in Southern Hemisphere, though there are no direct connections between TP and these signals in WAF.

Similar wave trains are found in observations. In Fig. 6b, a typical 200 hPa anomalous WAF in a cold TP year is illustrated to obtain a clearer picture of the observed wave train structures with the cold TP surface. Here the regression is

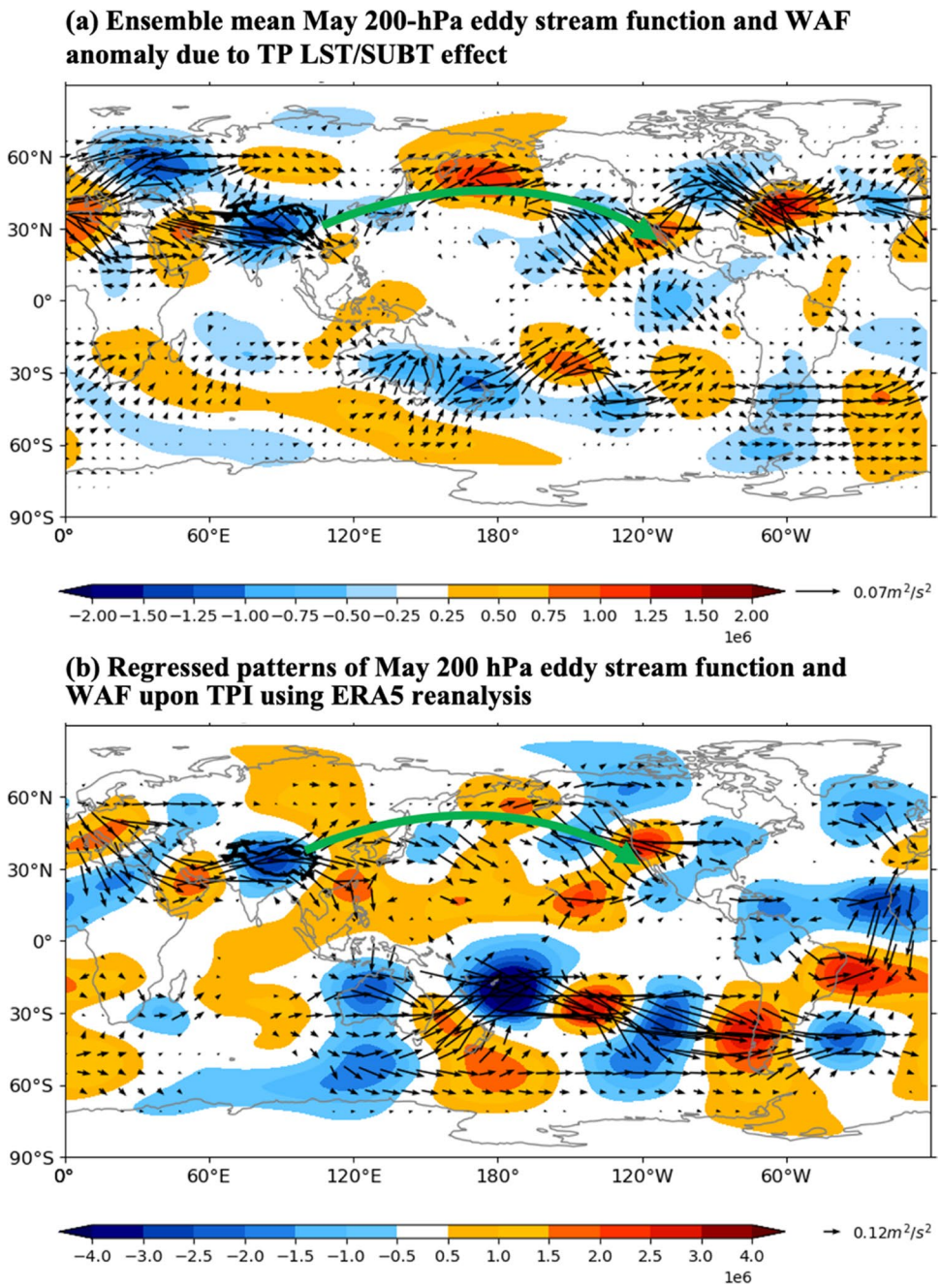


Fig. 6 **a** Ensemble mean of 200 hPa eddy stream function (color shading, unit: m^2/s) and corresponding wave activity flux (unit: m^2/s^2) responses in May to the TP LST/SUBT effect. **b** Regressed patterns of May 200 hPa eddy stream function and wave activity flux based on May TPI using ERA5 reanalysis data. Arrows in panels (**a**) and (**b**) denote the TRC wave train in LS4P-I model and in observations, respectively

applied to exhibit the typical wave train pattern with the TP surface forcing instead of showing the anomaly for a single year, as the patterns of eddy stream function and wave activity flux are relatively easier to be interfered by noises compared with other fields. The regressed patterns of the eddy stream function and WAF are calculated based on Tibetan Plateau Index (TPI), defined as the TP averaged 2 m surface air temperature (Xue et al. 2022). The observations show that with the cold TP surface, a similar wave train originating from the TP propagates eastward through the Bering Strait over the North Pacific Ocean to the west coast of the North America. From the west coast, the wave train also propagates southward and to the South America through the equator. However, in the midlatitudes of the Southern Hemisphere, the observed wave train pattern exhibits evident differences compared with the ensemble mean response of model simulations, suggesting the complexity of the cross hemispheric influence of the TP surface cooling.

In addition to the monthly mean (May) response of the wave train in terms of geopotential height in the upper level, the evolution of the wave train from May to June is also explored. Figure 7 shows the ensemble mean of the 20-day

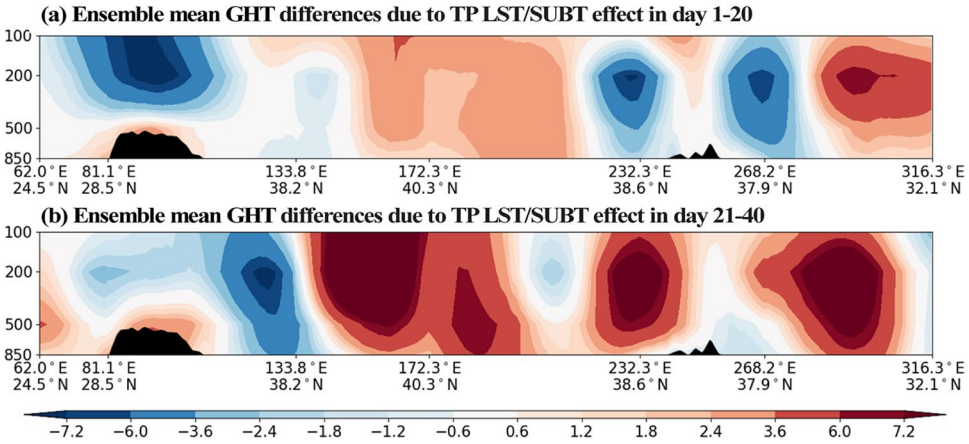


Fig. 7 Ensemble mean of the **a** day 1–20 and **b** day 21–40 averaged evolution of geopotential height differences (m) due to the TP LST/SUBT effect along the pathway of wave train from Tibetan Plateau to Rocky Mountain (purple line in Fig. 5)

averaged vertical-longitude cross section of the geopotential height responses. The cross section is selected along the pathway of the TRC wave train, which is marked by the purple line in Fig. 5. Comparing Figs. 5 and 7a, strong negative geopotential height anomalies are found above the whole TP. In its downstream regions, a positive geopotential height anomaly center in the central North Pacific and a negative anomaly center in the east North Pacific are also found. The vertical profiles of the above anomalies all exhibit a quasi-barotropic vertical structure. The above response patterns are consistent with the observed May geopotential height anomalies in 2003, though with a weaker magnitude (Fig. 8a) due to inter-model differences. Note that the cross section in Fig. 8a is not along the purple line in Fig. 5a, as in Fig. 7, but averaged over 30–42° N, which is mainly because the simulated pathway of the TRC wave train has shift in location compared with the observation.

In the next twenty days, the ensemble mean of the geopotential height anomaly still exhibits a horizonal structure like the TRC wave train but with some evolutions. One evolution is the phase change of the wave train around the Rocky Mountain with a positive geopotential height anomaly along the west coast and a negative anomaly in the downstream. Along with this, the strength of each action centers of the TRC wave train also exhibits variations. Around day 1–20, the action center above the TP is strongest, while during day 21–40, action centers over mid-east North Pacific and the western coast of North America are strong, implying a downstream development. Such wave train pattern is very similar to the observed geopotential height anomaly in June (Fig. 8b) as well, which explains why the model ensemble mean can simulate the observed June precipitation anomaly along the TRC wave train. The main difference is that the simulated atmospheric response in model ensemble evolve faster than the observation. The 20-day averaged TRC wave train evolution in the model mostly corresponds to the 30-day averaged evolution in the observation. In Figure S2, the ensemble mean of 30-day averaged TRC wave train evolution is also provided for comparison.

Such temporal scale discrepancy of atmospheric planetary waves between simulation and observation on S2S time scales is not rare as their periods are sensitive to the model success in reproducing mean state and external forcing (Brunet and Vautard 1996). In fact, in the last twenty days of the

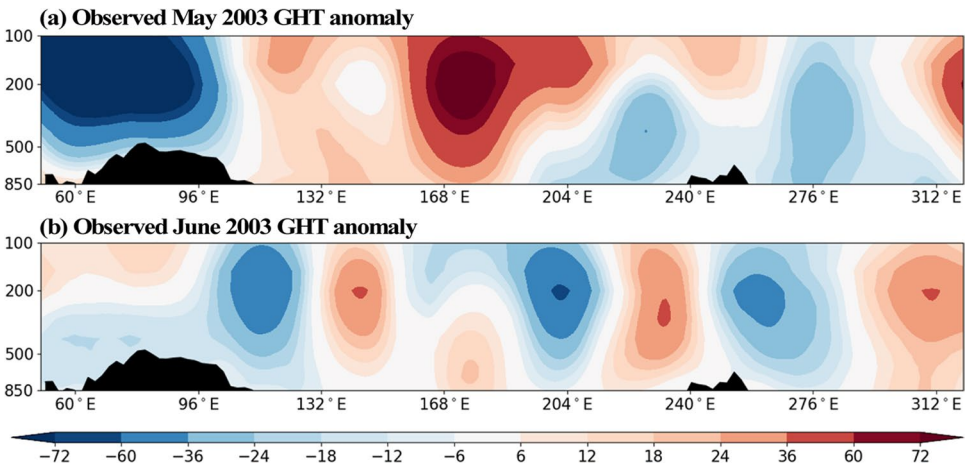


Fig. 8 Observed 30-day averaged geopotential height differences in 30–42°N from May 1st to June 29th between year 2003 and the climatology from ERA5 reanalysis data. The climatology is defined as the May–June average from 1981–2015. Note that the zonal mean is removed from the geopotential height

simulation, the wave train pattern from the central North Pacific to the North America is practically unchanged and closer to the observed pattern in June (results not shown), but with some phase differences upstream of the TP, which may explain at least in part the weak signal in the June precipitation anomaly in northeast Asia. From the evolution of the cross-section of the geopotential height along the wave train, we find that in both simulations and observations, TRC wave train is a vertically barotropic, slowly varying planetary scale wave train, usually with the phase changing period longer than one month.

4 Relationship between the TRC wave train and the T2m, precipitation anomalies

To further explore the TP's role and the influence of TRC wave train in S2S predictions, we check the response simulated by each model in May. In doing so, we find the simulated 200 hPa geopotential height differences due to the TP LST/SUBT effect in five of the LS4P-I models include a TRC wave train between the TP and North America with the phase and spatial structure consistent with the observations. Thus, all these five models produce the same sign of the response for most parts of the wave train. Similarly, we also find the five models for which the 200 hPa geopotential height differences either do not exhibit a wave train like structure or the wave train is not in the right phase from TP to the North America with the wave train over the TP and the Rocky Mountains showing the same phase. Figure 9 illustrates these inter-model contrasts by displaying the ensemble means of the 200 hPa geopotential height differences due to the TP LST/SUBT effect between the two groups of models. As shown in Fig. 9a, for the models that can reasonably simulate a TRC wave train, their ensemble mean shows a clear zonal wave-train structure consistent with the observation from TP to the North America (see Figs. 5b and 6b). For the models with a relatively poor wave train simulation (Fig. 9b) compared with the observation of 2003, their ensemble mean does not show a zonal wave train structure for most regions from TP to the eastern North Pacific. In the west of North America, a meridional triple structure emerges with the sign of geopotential height anomalies almost opposite to the observation.

Similarly, in Figs. 10 and 11 we compare the ensemble mean of May–June averaged T2m and June precipitation simulated by the two groups of models, respectively. It is evident that models with a better simulation of the TRC

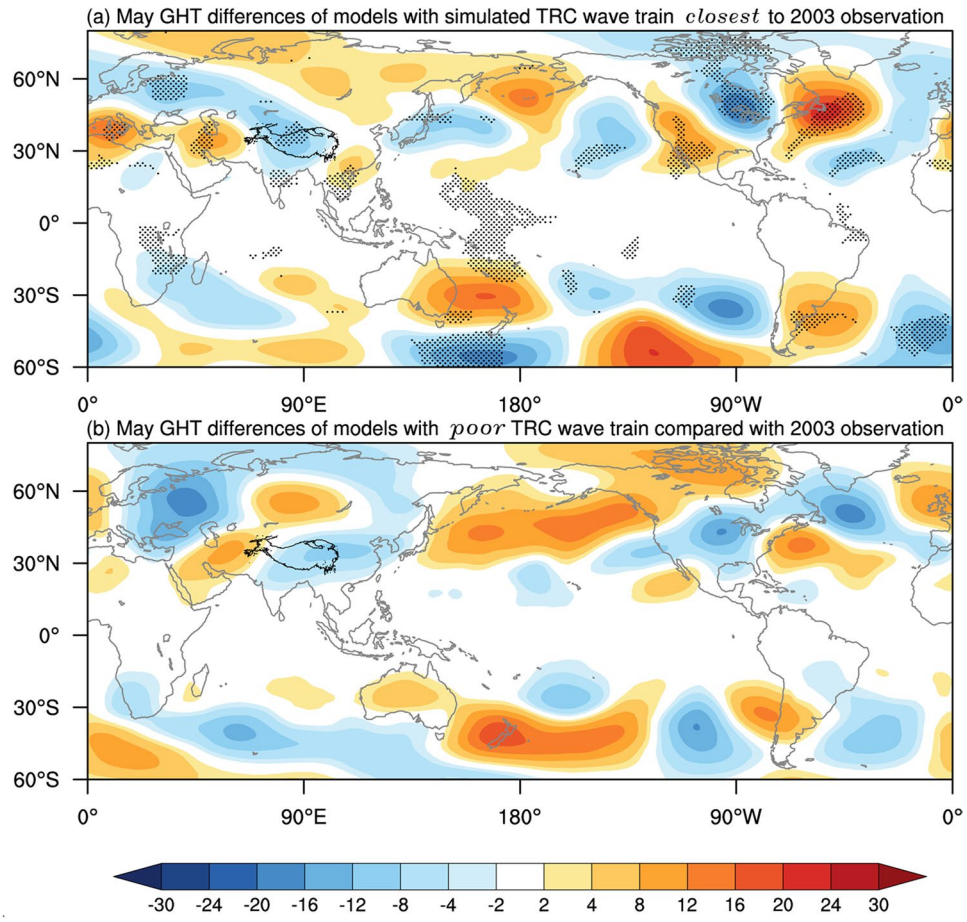


Fig. 9 Ensemble mean of May geopotential height (m) differences due to the TP LST/SUBT effect **a** for the 5 models with simulated TRC wave train closest to 2003 observation and **b** for the 5 models with relatively poor TRC wave train simulation compared with 2003 observation. In panel (**a**), black dots denote the areas where all the five models exhibit the same sign of response

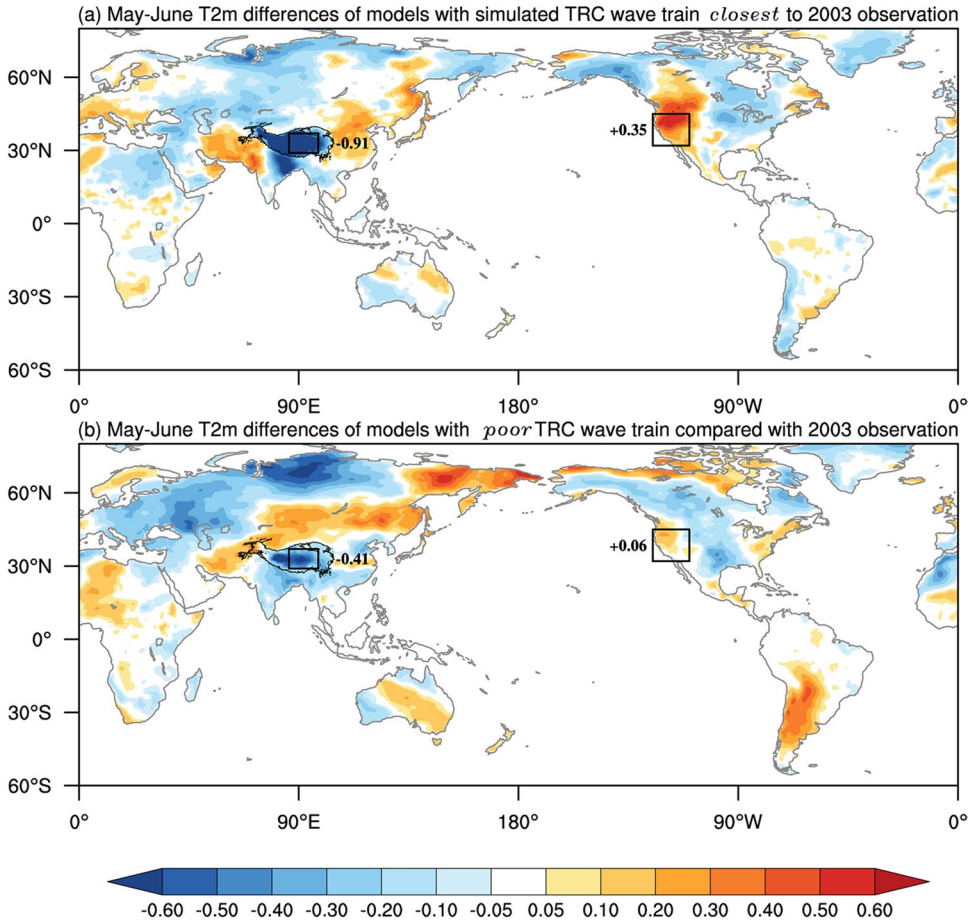


Fig. 10 Ensemble mean of May and June averaged 2 m air temperature (℃) differences due to the TP LST/SUBT effect **a** for the 5 models with simulated TRC wave train closest to 2003 observation and **b** for the 5 models with relatively poor TRC wave train compared with 2003 observation. Same as in Fig. 2, black boxes in panels (**a**) and (**b**) outline the main region of TP (29N-37N, 86-98E) and Rocky Mountain (32-45N, 110-125W) as defined in Xue et al. (2022), beside which values of the box averaged T2m anomaly are listed

wave train produce a May and June T2m anomaly closer to the observation, especially in northwest North America and southern Great Plains in the U.S., while those a poorer simulation of the wave train do not. This suggests that the TP surface cooling and the TRC wave train play a critical role in the T2m simulation in these regions for the case of 2003. However, there are still discrepancies and even T2m anomalies with opposite sign to the observed in the Indian peninsula compared with observations. A paper in this special issue (Saha et al. 2023) conjectures that the LST/SUBT effect in the western TP and Iranian Plateau play a dominant role for the Indian monsoon. Figure 11 also shows that June precipitations in the southern Yangtze River Basin, northwest North America, Great Plains in the U.S, central America and northern South America are closer to observations for models that can better simulate the wave train. In contrast, models with a relatively poor TRC wave train simulation compared with observations, greatly under-predict the precipitation anomalies in the above regions (Fig. 11b), especially in northwest North America. These results taking together suggest that the TRC wave train plays a key role in the influence of TP's surface and subsurface temperatures on the hot spot regions, especially for the regions in North America, though the detailed mechanisms through which the TRC wave train affects the precipitation in these different regions still need further investigations.

5 Wave trains from the TP into the Southern Hemisphere

In Section 3, we showed that the response to TP's surface cooling can extend to the atmospheric circulation in the Southern Hemisphere. In this section, we further explore this feature by examining each model's performance. We first select the NASA GEOS5 as an example and concentrate in the first two weeks' response to explore how the TP-induced wave train propagates into the Southern Hemisphere. The NASA GEOS5 not only simulates a TRC wave train close to the observation but also exhibits multiple pathways through which wave trains propagate across hemispheres. The model response is calculated as the daily difference between the EXP-CTL and EXP-LST/SUBT simulations, and averaged every two days to illustrate the pattern evolution.

As shown in Fig. 12, the initial response in the geopotential height to the cold TP surface in the selected model is cyclonic anomalous circulation over the TP, followed by a positive geopotential height anomaly downstream region in

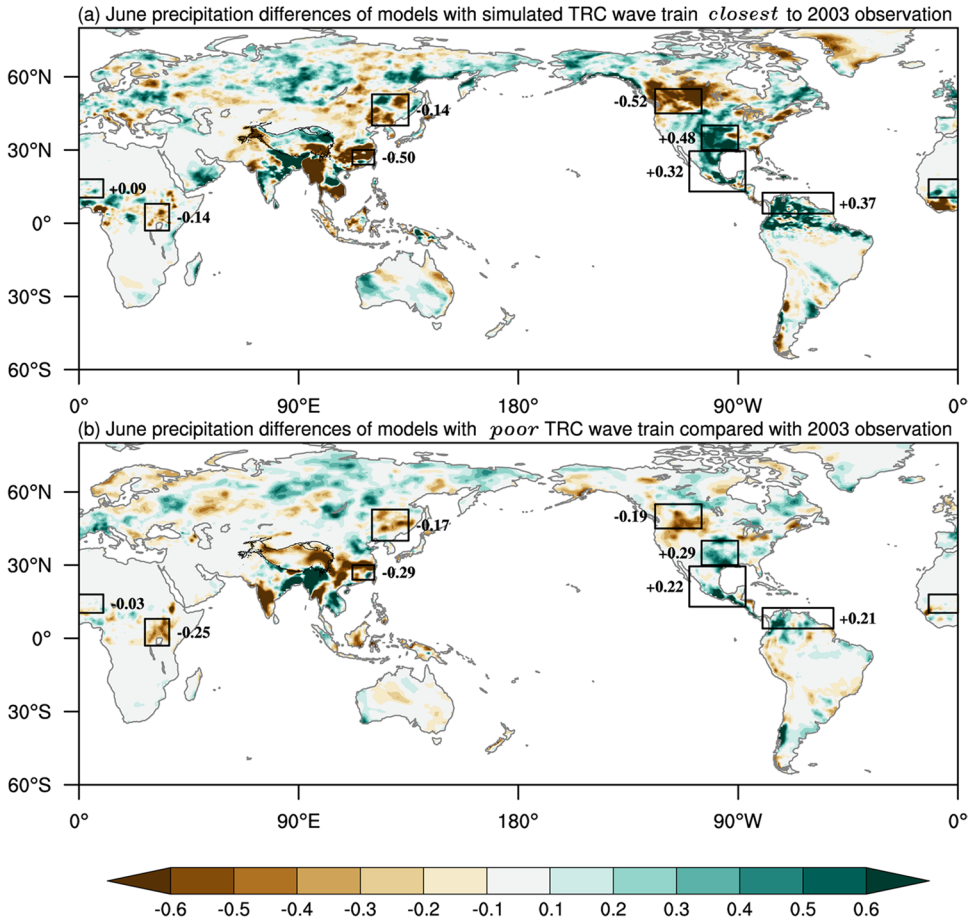


Fig. 11 Same as Fig. 10 but for June precipitation differences. Black boxes indicate the eight hot spot regions defined in Xue et al. (2022), with the box averaged precipitation differences listed beside

the first couple of days (Fig. 12a). In the subsequent two days, a wave-like structure with positive and negative anomalous centers extends from the TP through the northeast Asia to the Bering Strait (Fig. 12b). In day 5 and 6, geopotential height anomalies emerge over the west coast of North America. Anomalies are also noted at tropical latitudes and across the equator into the Southern Hemisphere. At least two pathways of wave like response in the atmospheric circulation emerge: one extending from the TP through Indonesia to Australia, while the other extending from the TP through central North Pacific to South Pacific (Fig. 12c). In day 7 and 8 (Fig. 12d), geopotential height responses acquire a more global character. The zonal wave-train-like response from TP to North America further develops equatorward along the west coast of this continent completing a TRC pattern. After day 7–8 (Fig. 12e–f), geopotential height responses are noted in the Southern Hemisphere, especially in the mid-high latitudes. Besides the two pathways along which the signal extends from the TP via either Indonesia or central Pacific to the Southern Hemisphere, the wave trains also extend along the west coast from North America to South America.

Therefore, from the initial responses of the 200 hPa geopotential height in NASA GEOS5 simulations, we can find that the atmospheric responses to the TP surface cooling can emerge almost immediately at the beginning 1–2 days over TP and the neighboring region, and form a TRC wave train response in a week; furthermore, the influence of TP's surface cooling can cross the equator and reach the Southern Hemisphere midlatitude in less than two weeks along multiple pathways with one from TP through Indonesia to Australia, one from TP through central North Pacific to central South Pacific, and one along the west coast from North America to South America.

Similar to Fig. 12, we have checked each model's initial response and find that the initial day-to-day response of the simulated geopotential height to the TP LST/SUBT effect in the models exhibits more pattern diversity in the Southern Hemisphere. Based on the region where a wave-train-structure response occurs, we can at least define three main wave train paths into the Southern Hemisphere from the model response: (1) Tibetan-Indian Ocean/Indonesia-South American wave train; (2) Tibetan-central Pacific-South American wave train and (3) Tibetan-North American-South American wave train, in which the TRC wave train can further extend southward along the west coast of America to the Southern Hemisphere. In Table 1, we list different situations of each model's initial two weeks' response in terms

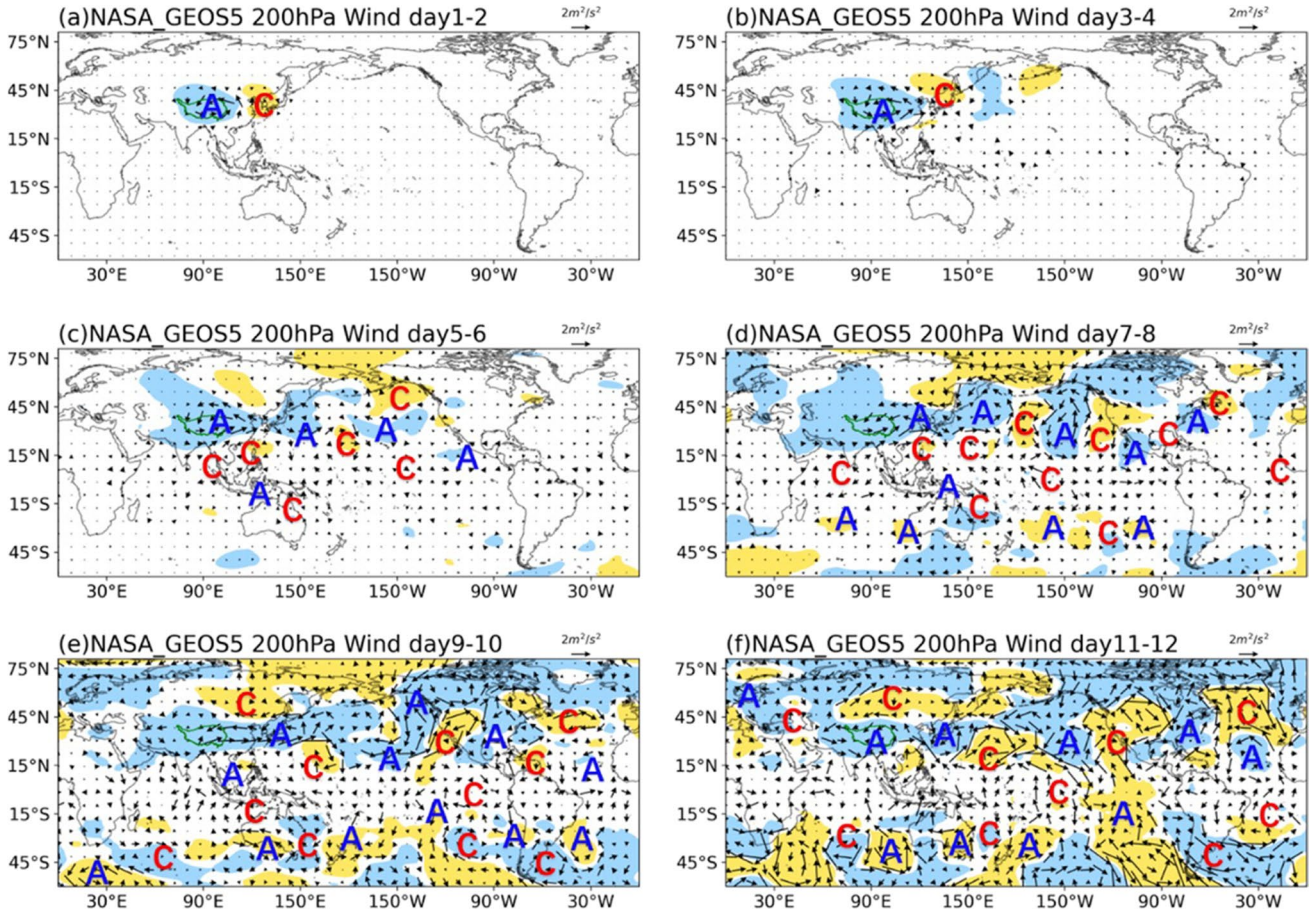


Fig. 12 Day-to-day response of the geopotential height to the Tibetan surface cooling to the TP LST/SUBT effect in NASA-GEOS5 model. Blue shadings denote the regions with geopotential height anomalies less than -0.1 gpm, and yellow shadings denote the regions with geopotential height anomalies over 0.1 gpm. Red capital letter A represents anticlockwise anomalous circulation and blue capital letter C represents negative clockwise anomalous circulation (Note that, to avoid any confusion from the different sign of the Coriolis parameter, we use clockwise/anticlockwise instead of the conventional cyclonic/anticyclonic to denote the direction of atmospheric circulations). Green lines with arrows indicate possible pathways of the wave train

of the above three wave trains except for the JMA CPS2 model, which does not provide daily data. Large diversities exist among models for the three pathways from TP to the Southern Hemisphere. Most models can only detect one or two types of pathways to the Southern Hemisphere. For some model, no pathways of wave train to the Southern Hemisphere can be detected, though there are also response in the geopotential height there as well. Given the difficulties in identifying wave propagation across the equator (Li et al. 2019), the detection of the wave train also exists uncertainties. In Table 1, we also roughly list the confidence/uncertainty in identifying the different wave trains, based on the evidence of each action center (cyclonic and anticyclonic centers) along the pathway to judge whether there exists uncertainty. It is evident that there are strong inter-model discrepancies in simulating the cross-hemispheric propagation of wave trains. The associated diversities in the model response in the Southern Hemispheric circulations could be one of the main reasons that the simulated response exhibit great inconsistency with the observation, though the model ensembles show strong Southern Hemispheric responses especially in the mid-high latitudes.

6 Conclusions

This study has investigated the mechanisms of the global atmospheric response to the TP spring LST/SUBT anomalies in simulations by LS4P-I ESMs. The model ensemble shows that the simulations with the TP LST/SUBT initialization procedure described by Xue et al. (2021) can produce persistent TP cold surface anomaly in May and June, as it was observed in 2003. The cold TP results in negative geopotential height anomalies and cyclonic anomalous circulations in the upper troposphere over the TP. The ensemble model simulations show that, with the strong westerly jet

Table 1 Transient wave train response (first two weeks' response) to TP LST/SUBT effects in each model

Model	Tibetan-Indian Ocean-South America wave train	Tibetan-Central Pacific Ocean-South America wave train	Tibetan-North America-South America Wave train
ACCESS-S2	-	-	-
AFES-HU	-	✓✓	-
CAS-ESM	✓	✓✓	-
FGOALS-f2	✓✓	✓✓	✓✓
CFS/SSiB2	✓✓	✓✓	✓
CMCC-SPS3	-	✓	✓
CNRMAMIP	✓	✓✓	-
CNRMCMIP	✓✓	✓	-
ECMWF	✓	✓	-
E3SM	✓	✓	-
GRAPES	✓	-	-
IITMCFS	✓✓	✓✓	✓
JMA CPS2	-	-	-
KIM HR	✓✓	✓✓	✓✓
KIM LR	✓	✓✓	✓✓
NASAGEOS5	✓✓	✓	✓

✓✓ : likely to generate a wave train response

✓ : possible to have wave train response but with large uncertainty

- : no evidence of wave train response observed

across the extratropical Asian-Pacific region, the TP surface cooling generates a barotropic, persistent (evolving in time scales longer than a month) TRC wave train from TP through northeast Asia and Bering Strait to the west part of the North America, whose features closely resemble the observed geopotential height anomaly from May to June in 2003. These results indicate that the TP spring surface cooling is a first order factor for the observed spring to early summer circulation anomaly from the TP to the Rocky Mountain in year 2003.

The LS4P-I simulations further show that the TP surface thermal state not only has circumglobal influence in the Northern Hemisphere, but it also affects the extratropical atmospheric circulation in the Southern Hemisphere, though with a large uncertainty due to inter-model variability. The model ensemble shows that the TP generated TRC wave train, after reaching the west part of the North America, extends further across the equator to the west part of South America. The initial response of LS4P-I model to the TP LST/SUBT effect also suggests that, in addition to the path along the western America, the TP surface cooling may also affect the Southern Hemisphere via other pathways (i.e., from TP via Indonesia to Australia, and from TP via central North Pacific to South Pacific). Although cross-equator interactions are observed in the tropics for daily synoptic flow (e.g., Hoskins et al. 2020; Hoskins and Yang 2021) and interhemispheric influence of the northern summer monsoon has been conjectured on the southern subtropical anticyclones (Lee et al. 2013), the TP's influence on the southern mid- and high-latitudes on S2S time scale has not been clearly pointed out before. Further investigations are required to narrow down further on the mechanisms at work for such interhemispheric teleconnections.

It is well known and extensively studied that the TP surface thermal state can significantly influence the weather and climate in East Asia (e.g. Liu et al. 2020). The LS4P-I experiment, however, shows that the TP surface anomaly can result in persistent and global scale anomalies in atmospheric circulations, and has a near-global influence on the summer T2m and precipitation on S2S time scale. Furthermore, the LS4P-I experiment confirms and highlights the important even critical role of the TRC wave train in the global influence of the TP surface anomaly. The analysis of 16 state-of-the-art ESMs shows for the first time that the springtime TP surface anomaly can modulate a persistent quasi-barotropic TRC wave train. Most of the hot spots (six of the eight) of TP's influence identified in Xue et al. (2022, 2023) are located along the wave train. The LS4P-I models that produce a better simulation of the TRC wave produce T2m and June precipitation anomalies closer to the observation in June. The models that produce a poorer TRC wave train greatly under-predict the T2m and precipitation anomalies, especially in the northwest of North America and the southern Great Plains. In another study, Qin et al. (2024) using two ESMs participating in the LS4P-I shows that the S2S prediction skill of the summer precipitation can be significantly improved if a nudging technique is applied to the wind fields to better initialize the TRC wave train. Combined with our study, the importance of TRC wave train in the S2S prediction using TP surface anomaly is systematically explored and identified in the first phase experiment of the LS4P project.

Earlier studies have shown that, in summertime, there exists a circumglobal teleconnection pattern (CTP) in the extra-tropics of the Northern Hemisphere along the westerly jet. The latent heat with the strong convective monsoon precipitation is suggested a major driver for the CTP (e.g. Lau and Peng 1991; Lau and Weng 2002; Lau et al. 2004; Ding and Wang 2005; Ding et al. 2011). In springtime, however, there is no strong convective monsoon precipitation in the extra-tropics. Therefore, the TRC wave train identified in LS4P-I, which is prominent mainly in May and June, must be driven by different factors thus with different dynamical characteristics. The LS4P-I experiment has shown that the TP surface forcing can generate the TRC wave train, and the wave train seems further enhanced and propagate downstream and southward to the Southern Hemisphere when reaching the Rocky Mountain. Even though, it remains unclear whether the surface forcing from the high mountains (i.e. TP and Rocky Mountain) is the key driver

of the TRC wave train behavior and to what extent the high mountain forcing can affect the formation, evolution, phase and extension of the wave train. These questions will be further explored in the Second Phase experiment of the LS4P project, in which the separate and the joint influences of the TP and Rocky Mountain surface forcing on the global atmospheric circulations will be systematically investigated.

In our study, we show that the TP land surface anomaly, via the land-atmosphere interaction, can affect the large-scale atmospheric circulations thus has a global impact on the air temperature and precipitation on S2S time scales. We've noticed that some recent study also reports that anomalous TP sensible heating in summer could trigger hemispherical climate responses as well via longer time air-sea interactions (Xie et al. 2023). Therefore, the global influence of the TP thermal state may cover various time scales by complicated air-land-ocean interactions, the detailed processes of which need to be further delineated.

In addition, though our study shows the importance of the springtime TP surface anomaly for the S2S variability in some regions over the globe, it is still an open question as to the cause of the TP surface anomaly. As suggested in Zhang et al. (2019), the TP surface anomaly in spring is closely related to the variation in extratropical atmospheric circulations and the snow fall in preceding months. However, it remains unclear whether such variation in atmospheric circulations is caused by external forcings or mainly the behavior of atmospheric internal variabilities. This question will be explored in future studies.

Supplementary Information The online version contains supplementary material available at https://doi.org/10.1007/s00382-024-07210-5.

Acknowledgements The authors sincerely thank the two anonymous reviewers for their constructive suggestions, which greatly helped improve the quality of the manuscript. We sincerely thank Zhijiong Cao for her help in conducting the significance test. LS4P is a GEWEX project under the auspices of the World Climate Research Programme (WCRP). Each LS4P model group's efforts are supported by the participants' home institutions and/or funding agencies. We thank the support of the Strategic Priority Research Program of Chinese Academy of Sciences under Grant XDA201030804 and the support of U.S. National Science Foundation Grant AGS-1849654.

Funding Strategic Priority Research Program of Chinese Academy of Sciences, XDA201030804, Yang Zhang, U.S. National Science Foundation Grant, AGS1849654,Yongkang Xue

Data availability The LS4P simulation data analyzed in this study can be downloaded upon request to Yongkang Xue (yxue@geog.ucla.edu). Also, all simulation datasets are available from http://data.tpdc.ac.cn/en/. See Xue et al. (2021) for data access and download instructions. The observational datasets were downloaded from open sources. The CMA observational datasets are available from http://data.cma.cn/en. CRU datasets are available from https://crudata.uea.ac.uk/cru/data/hrg/cru_ts_4.02/. CAMS datasets are available from https://psl.noaa.gov/data/gridded/data.ghcncams.html. The ERA5 reanalysis data are available from https://www.ecmwf.int/en/forecasts/dataset/ecmwf-reanalysis-v5. The high-resolution topography dataset was downloaded from SRTM30_PLUS https://topex.ucsd.edu/WWW_html/srtm30_plus.html (Becker et al. 2009), which was developed from a wide variety of data sources including satellite radar.

Declarations

Conflicts of interests The authors have no relevant financial or non-financial interests to disclose.

Open Access This article is licensed under a Creative Commons Attribution 4.0 International License, which permits use, sharing, adaptation, distribution and reproduction in any medium or format, as long as you give appropriate credit to the original author(s) and the source, provide a link to the Creative Commons licence, and indicate if changes were made. The images or other third party material in this article are included in the article's Creative Commons licence, unless indicated otherwise in a credit line to the material. If material is not included in the article's Creative Commons licence and your intended use is not permitted by statutory regulation or exceeds the permitted use, you will need to obtain permission directly from the copyright holder. To view a copy of this licence, visit http://creativecommons.org/licenses/by/4.0/.

References

Bao Q, Wu X, Li J, He B, Wang X, Liu Y, Wu G (2019) Outlook for El Niño and the Indian Ocean Dipole in autumn-winter 2018–2019. Chinese Sci Bull 64:73–78. https://doi.org/10.1360/N972018-00913

Becker JJ, Sandwell DT, Smith WHF, Braud J, Binder B, Depner JL, ... Weatherall P (2009) Global bathymetry and elevation data at 30 arc seconds resolution: SRTM30_PLUS. Mar Geod 32(4):355–371

Brunet G, Vautard R (1996) Empirical normal modes versus empirical orthogonal functions for statistical prediction. J Atmos Sci 53:3468–3489

Chan D, Zhang Y, Wu Q, Dai X (2020) Quantifying the dynamics of the interannual variabilities of the wintertime East Asian Jet Core. Clim Dyn 54:2447–2463. https://doi.org/10.1007/s00382-020-05127-3

Chen J, Ma Z, Li Z, Shen X, Su Y, Chen Q, Liu Y (2020) Vertical diffusion and cloud scheme coupling to the Charney-Phillips vertical grid in GRAPES global forecast system. Q J Roy Meteor Soc 146:2191–2204. https://doi.org/10.1002/qj.3787

Ding Q, Wang B (2005) Circumglobal teleconnection in the Northern Hemisphere summer. J Climate 18:3483–3505

Ding Q, Wang B, Wallace JM, Branstator G (2011) Tropical-extratropical teleconnections in boreal summer: observed interannual variability. J Climate 24:1878–1896

Fan Y, van den Dool H (2008) A global monthly land surface air temperature analysis for 1948–present. J Geophys Res 113:D01103

Gillett ZE, Hendon HH, Arblaster JM, Lin H, Fuchs D (2022) On the dynamics of Indian Ocean Teleconnections into the Southern Hemisphere during Austral Winter. J Atmos Sci 79:1520–469

Golaz J-C, Caldwell PM, Van Roekel LP et al (2019) The DOE E3SM coupled model version 1: overview and evaluation at standard resolution. J Adv Model Earth Sy 113:D01103. https://doi.org/10.1029/2018MS001603

Harris I, Jones PD, Osborn TJ, Lister DH (2014) Updated high-resolution grids of monthly climatic observations – the CRU TS3.10 Dataset. Int J Climatol 34:623–642. https://doi.org/10.1002/joc.3711

Harris I, Osborn TJ, Jones P, Lister D (2020) Version 4 of the CRU TS monthly high-resolution gridded multivariate climate dataset. Sci Data 7(1):109

Hersbach H, Bell B, Berrisford P, Hirahara S, Horányi A, Muñoz-Sabater J, ... Thépaut JN (2020) The ERA5 global reanalysis. Q J R Meteorol Soc 146(730):1999–2049

Hong S-Y, Kwon Y, Kim T-H, Kim J-EE, Choi S-J, Kwon I-H, Kim J, Lee E-H, Park R-S, Kim D-I (2018) The Korean Integrated Model (KIM) system for global weather forecasting, Asia-Pacific. J Atmos Sci 54:267–292. https://doi.org/10.1007/s13143-018-0028-9

Hong S-Y, Park H, Cheong H-B, KIM, J-E E, Koo, M-S, Jang J, Ham, S, Hwang, S-O, Park, B-K, Chang, E-C, and Li, H, (2013) The global/regional integrated model system (GRIMs). Asia-Pacific J Atmos Sci 49:219–243. https://doi.org/10.1007/s13143-013-0023-0

Hoskins BJ, Yang G-Y, Fonseca RM (2020) The detailed dynamics of the June–August Hadley Cell. Q J R Meteorol Soc 146(727):557–575. https://doi.org/10.1002/qj.3702

Hoskins BJ, Yang GY (2021) The detailed dynamics of the Hadley Cell. Part 2: December to February. J Clim 34(2):805–823. https://doi.org/10.1175/JCLI-D-20-0504.1

Jiang Y, Yang X, Liu X, Yang D, Sun X, Wang M, Ding A, Wang T, Fu C (2017) Anthropogenic aerosol effects on East Asian winter monsoon: the role of black carbon-induced Tibetan Plateau warming. J Geophys Res Atmos 122:5883–5902. https://doi.org/10.1002/2016JD026237

Johnson SJ, Stockdale TN, Ferranti L, Balmaseda MA, Molteni F, Magnusson L, Tietsche S, Decremer D, Weisheimer A, Balsamo G, Keeley SPE, Mogensen K, Zuo H, Monge-Sanz BM (2019) SEAS5: the new ECMWF seasonal forecast system. Geosci Model Dev 12:1087–1117. https://doi.org/10.5194/gmd-12-1087-2019

Lau WKM, Peng L (1991) Dynamics of Atmospheric Teleconnections during the Northern summer. J Clim 2:140–158

Lau WKM, Weng H (2002) Recurrent teleconnection patterns linking summertime precipitation variability over East Asia and North America. J Meteorol Soc Jpn 80:1309–1324

Lau WKM, Lee JY, Kim KM, Kang IS (2004) The North Pacific as a regulator of summertime climate over Eurasian and North America. J Clim 17:819–833

Lee S, Mechoso CR, Wang C, Neelin JD (2013) Interhemispheric Influence of the Northern Summer Monsoons on Southern Subtropical Anticyclones. J Clim 26:10193–10204

Lee J, Xue Y, De Sales F, Diallo I, Marx L, Ek M, Sperber KR, Gleckler PJ (2019) Evaluation of multi-decadal UCLACFSv2 simulation and impact of interactive atmospheric-ocean feedback on global and regional variability. Clim Dyn 52:3683–3707. https://doi.org/10.1007/s00382-018-4351-8

Li Y, Lu R, Dong B (2007) The ENSO–Asian monsoon interaction in a coupled ocean–atmosphere GCM. J Climate 20(20):5164–5177

Li T, Wang B, Wu B, Zhou T, Chang C, Zhang R (2017) Theories on formation of an anomalous anticyclone in western North Pacific during El Nino: a review. J Meteorol Res 31:987–1006

Li Y, Feng J, Li J, Hu A (2019) Equatorial windows and barriers for stationary Rossby Wave Propagation. J Climate 32:6117–6135

Lin Z-H, Yu Z, Zang H, Wu C-L (2016) Quantifying the attribution of model bias in simulating summer hot days in China with IAP AGCM 4.1. Atmos Ocean Sci Lett 9:436–442

Liu YM, Lu M, Yang H, Duan A, He B, Yang S, Wu G (2020) Land–atmosphere–ocean coupling associated with the Tibetan Plateau and its climate impacts. Natl Sci Rev 7(3):534–552. https://doi.org/10.1093/nsr/nwaa011

MacLachlan C, Arribas A, Peterson D, Maidens A, Fereday D, Scaife AA, Gordon M, Vellinga M, Williams A, Comer RE, Camp J, Xavier P, Madec G (2015) Global Seasonal forecast system version 5 (GloSea5): a high-resolution seasonal forecast system. Q J Roy Meteor Soc 141:1072–1084. https://doi.org/10.1002/qj.2396

Merryfield WJ, Baehr J, Batté L, Becker EJ, Butler AH, Coelho CAS, Danabasoglu G, Dirmeyer PA, Doblas-Reyes FJ, Domeisen DIV, Ferranti L, Ilynia T, Kumar A, Müller WA, Rixen M, Robertson AW, Smith DM, Takaya Y, Tuma M, Vitart F, White CJ, Alvarez MS, Ardilouze C, Attard H, Baggett C, Balmaseda MA, Beraki AF, Bhattacharjee PS, Bilbao R, de Andrade FM, DeFlorio MJ, Díaz LB, Ehsan MA, Fragkoulidis G, Grainger S, Green BW, Hell MC, Infanti JM, Isensee K, Kataoka T, Kirtman BP, Klingaman NP, Lee J-Y, Mayer K, McKay R, Mecking JV, Miller DE, Neddermann N, Justin Ng CH, Ossó A, Pankatz K, Peatman S, Pegion K, Perlwitz J, Recalde-Coronel GC, Reint- ges A, Renkl C, Solaraju-Murali B, Spring A, Stan C, Sun YQ, Tozer CR, Vigaud N, Woolnough S, Yeager S (2020) Current and emerging developments in subseasonal to decadal prediction. Bull Am Meteorol Soc 101: E869–E896. https://doi.org/10.1175/BAMS-D-19-0037.1

Molod A, Hackert E, Vikhliaev Y, Zhao B, Barahona D, Vernieres G, Borovikov A, Kovach RM, Marshak J, Schubert S, Li Z, Lim Y-K, Andrews LC, Cullather R, Koster R, Achuthavarier D, Carton J, Coy L, Freire JLM, Longo KM, Nakada K, Pawson S (2020). GEOS-S2S Version 2: the GMAO high resolution coupled model and assimilation system for seasonal prediction. J Geophy Res-Atmos 125:e2019JD031767. https://doi.org/10.1029/2019JD031767

Nakamura T, Yamazaki K, Iwamoto K, Honda M, Miyoshi Y, Ogawa Y, Ukita J (2015) A negative phase shift of the winter AO/NAO due to the recent Arctic sea-ice reduction in late autumn J Geophys Res-Atmos 120:3209–3227. https://doi.org/10.1002/2014JA020764

Nie Y, Zhang Y, Chen G, Yang X-Q (2016) Delineating the barotropic and baroclinic mechanisms in the midlatitude eddy-driven jet response to lower-tropospheric thermal forcing. J Atmos Sci 73:429–448. https://doi.org/10.1175/JAS-D-15-0090.1

Qin Y, Tang Q, Xue Y, Liu Y, Lin Y (2024) Improved subseasonal-to-seasonal precipitation prediction of climate models with nudging approach: better initialization of Tibetan Plateau- Rocky mountain circumglobal wave train and land surface conditions. Clim Dyn. https://doi.org/10.1007/s00382-023-07082-1

Robertson AW, Camargo SJ, Sobel A, Vitart F, Wang S (2018) Summary of workshop on sub-seasonal to seasonal predictability of extreme weather and climate. npj Clim Atmos Sci 1:20178, https://doi.org/10.1038/s41612-017-0009-1

Saha SK, Sujith K, Pokhrel S, Chaudhari HS, Hawra A (2017) Effect of multilayer snow scheme on the simulation of the snow: Offline Noah and coupled with NCEPCFSv2. J Adv Model Earth Sy 9:271–290. https://doi.org/10.1002/2016MS000845

Saha SK, Xue Y, Krishnakumar S, Diallo I, Shivamurthy Y, Nakamura T, Tang Q, Chaudhari HS (2023). A dominant mode in the first phase of the Asian summer monsoon rainfall: role of antecedent remote land surface temperature. Clim Dynam 1–17. https://doi.org/10.1007/s00382-023-06709-7

Sanna A, Borrelli A, Athanasiadis P, Materia S, Storto A, Navarra A, Tibaldi S, Gualdi S (2016) CMCC-SPS3: the CMCC Seasonal Prediction System 3. CMCC Research Paper (RP0285), available at: https://www.cmcc.it/wp-content/uploads/2017/12/rp0285-csp-10-2017.pdf

Takaya K, Nakamura H (2001) A formulation of a phase-independent wave-activity flux for stationary and migratory quasigeostrophic eddies on a zonally varying basic flow. J Atmos Sci 58:608–627. https://doi.org/10.1175/1520-0469(2001)058%3c0608:AFOAPI%3e2.0.CO;2

Takaya Y, Hirahara S, Yasuda T, Matsueda S, Toyoda T, Fujii Y, Sugiomoto H, Matsukawa C, Ishikawa I, Mori H, Nagasawa R, Kubo Y, Adachi N, Yamanaka G, Kuragano T, Shimpo A, Maeda S, Ose T (2018) Japan Meteorological Agency/Meteorological Research Institute-Coupled Prediction System version 2 (JMA/MRI-CPS2): atmosphere-land-ocean-sea ice coupled prediction

system for operational seasonal forecasting. Clim Dynam 50:751–765. https://doi.org/10.1007/s00382-017-3638-5

Tang Q, Klein SA, Xie S, Lin W, Golaz J-C, Roesler EL, Taylor MA, Rasch PJ, Bader DC, Berg LK, Caldwell P, Giangrande SE, Neale RB, Qian Y, Riihimaki LD, Zender CS, Zhang Y, Zheng X (2019) Regionally refined test bed in E3SM atmosphere model version 1 (EAMv1) and applications for high-resolution modelling. Geosci Model Dev 12:2679–2706. https://doi.org/10.5194/gmd-12-2679-2019

Voldoire A, Saint-Martin D, Sénési S, Decharme B, Alias A, Chevallier M, Colin J, Guérémy J-F, Michou M, Moine M-P, Nabat P, Roehrig R, Salas y Mélia D, Séférian R, Valcke S, Beau I, Belamari S, Berthet S, Cassou C, Cattiaux J, Deshayes J, Douville H, Ethé C, Franchistéguy L, Geoffroy O, Lévy C, Madec G, Meurdesoif Y, Msadek R, Ribes A, Sanchez-Gomez E, Terray L, Waldman R, (2019) Evaluation of CMIP6 DECK experiments with CNRM-CM6-1. J Adv Model Earth Sy 11:2177–2213

Vitart F (2017) Madden–Julian oscillation prediction and teleconnections in the S2S database. Quart J Roy Meteor Soc 143:2210–2220. https://doi.org/10.1002/qj.3079

Wang B, Wu R, Fu X (2000) Pacific-East Asian teleconnection: how does ENSO affect East Asian climate? J Climate 13:1517–1536

Woolnough SJ (2019) The Madden-Julian oscillation. In: Robertson AW, Vitart F (eds) Sub-Seasonal to seasonal prediction: the gap between weather and climate forecasting. Elsevier, pp 93–117

Xie Y, Huang J, Wu G, Liu Y, Dong W, Lu M, He B, Su Z, Bao Q, Zhao Q, Liu Y (2023) Oceanic repeaters boost the global climatic impact of the Tibetan Plateau. Sci Bull 68(19):2225–2235. https://doi.org/10.1016/j.scib.2023.07.019

Xue Y, Juang H-MH, Li W-P, Prince S, DeFries R, Jiao Y, Vasic R (2004) Role of land surface processes in monsoon development: East Asia and West Africa. J Geophys Res-Atmos 109:D03105. https://doi.org/10.1029/2003JD003556

Xue Y, Oaida CM, Diallo I, Neelin JD, Li S, De Sales F, Gu Y, Robinson DA, Vasic R, Yi L (2016) Spring land temperature anomalies in northwestern US and the summer drought over Southern Plains and adjacent areas. Environ Res Lett 11:044018. https://doi.org/10.1088/1748-9326/11/4/044018

Xue Y, Diallo I, Li W, Neelin JD, Chu PC, Vasic R, Guo W, Li Q, Robinson DA, Zhu Y, Fu C, Oaida CM (2018) Spring land surface and subsurface temperature anomalies and subsequent downstream late spring-summer droughts/floods in North America and East Asia. J Geophys Res 105:5001–5019. https://doi.org/10.1029/2017JD028246

Xue Y, Diallo I, Boone AA, Yao T, Zhang Y, Zeng X, Neelin JD, Lau WKM, Pan Y, Liu Y, Pan X, Tang Q, Van Oevelen PJ, Sato T, Koo M-S, Materia S, Shi C, Yang J, Ardilouze C, Lin Z, Xin Q, Nakamura T, Saha SK, Senan R, Takaya Y, Wang H, Zhang H, Zhao M, Nayak HP, Chen Q, Feng J, Brunke MA, Fan T, Hong S, Nobre P, Peano D, Qin Y, Vitart F, Xie S, Zhan Y, Klocke D, Leung R, Li X, Ek M, Guo W, Balsamo G, Bao Q, Chou SC, Rosnay PD, Lin Y, Zhu Y, Qian Y, Zhao P, Tang J, Liang X-Z, Hong J, Ji D, Ji Z, Qiu Y, Sugimoto S, Wang W, Yang K, Yu M (2022) Spring land temperature in Tibetan Plateau and Global-Scale Summer precipitation – initialization and improved prediction. Bull Am Meteorol Soc 103:12. https://doi.org/10.1175/BAMS-D-21-0270.1,E2756-E2767

Xue Y, Yao T, Boone AA, Diallo I, Liu Y, Zeng X, Lau WKM, Sugimoto S, Tang Q, Pan X, Van Oevelen PJ, Klocke D, Koo M–S, Lin Z, Takaya Y, Sato T, Ardilouze C, Saha SK, Zhao M, Liang X–Z, Vitart F, Li X, Zhao P, Neelin JD, Guo W, Yu M, Qian Y, Shen SSP, Zhang Y, Yang K, Leung R, Yang J, Qiu Y, Brunke MA, Chou SC, Ek M, Fan T, Guan H, Lin H, Liang S, Materia S, Nakamura T, Qi X, Senan R, Shi C, Wang H, Wei H, Xie S, Xu H, Zhang H, Zhan Y, Li W, Shi X, Nobre P, Qin Y, Dozier J, Ferguson CR, Balsamo G, Bao Q, Feng J, Hong J, Hong S, Huang H, Ji D, Ji Z, Kang S, Lin Y, Liu W, Muncaster R, Pan Y, Peano D, Rosnay PD, Takahashi HG, Tang J, Wang G, Wang S, Wang W, Zhou X, Zhu Y (2021) Impact of initialized land surface temperature and snowpack on subseasonal to seasonal prediction project, phase I (LS4P-I): organization and experimental design. Geosci Model Dev 14:1-30

Xue Y, Diallo I, Boone AA, Zhang Y, Zeng X, Lau WKM, David Neelin J, Yao T, Tang Q, Sato T, Koo M-S, Vitart F, Ardilouze C, Saha SK, Materia S, Lin Z, Takaya Y, Yang J, Nakamura T, Qi X, Qin Y, Nobre P, Senan R, Wang H, Zhang H, Zhao M, Nayak HP, Pan Y, Pan X, Feng J, Shi C, Xie S, Brunke MA, Bao Q, Bottino MJ, Fan T, Hong S, Lin Y, Peano D, Zhan Y, Mechoso CR, Ren X, Balsamo G, Chou SC, de Rosnay P, van Oevelen PJ, Klocke D, Ek M, Li X, Guo W, Zhu Y, Tang J, Liang X-Z, Qian Y, Zhao P (2023) Remote effects of Tibetan Plateau spring land temperature on global subseasonal to seasonal precipitation prediction and comparison with effects of sea surface temperature - The GEWEX/LS4P Phase I experiment. Clim Dyn. https://doi.org/10.1007/s00382-023-06905-5

Zhang Y, Zou T, Xue Y (2019) An Arctic-Tibetan connection on subseasonal to seasonal time scale. Geophys Res Let 46:2790–2799

Publisher's Note Springer Nature remains neutral with regard to jurisdictional claims in published maps and institutional affiliations.

Authors and Affiliations

Yang Zhang[1] · Yan Pan[1,2] · Yongkang Xue[3] · Ismaila Diallo[4] · Xubin Zeng[5] · Shuting Li[1] · J. David Neelin[3] · William K. M. Lau[6] · Aaron A. Boone[7] · Frederic Vitart[8] · Tandong Yao[9] · Qi Tang[10] · Tomonori Sato[11] · Myung-Seo Koo[12] · Constantin Ardilouze[7] · Subodh K. Saha[13] · Jing Yang[14] · Stefano Materia[15] · Zhaohui Lin[16] · Xin Qi[14] · Yi Qin[17] · Tetsu Nakamura[11] · Paulo Nobre[18] · Daniele Peano[19] · Retish Senan[8] · Yuhei Takaya[20] · Hailan Wang[21] · Hongliang Zhang[22] · Yanling Zhan[16] · Mei Zhao[23] · Carlos R. Mechoso[3] · Qing Bao[24] · Marcus Jorge Bottino[18] · Songyou Hong[11,25] · Yanluan Lin[26] · Shaocheng Xie[10] · Xiaoduo Pan[9] · Hara Prasad Nayak[3] · Sin Chan Chou[18] · Weidong Guo[1]

✉ Yang Zhang
yangzhang@nju.edu.cn

✉ Yongkang Xue
yxue@geog.ucla.edu

1 School of Atmospheric Sciences, Nanjing University, Nanjing, China

2 Duke University, Durham, NC, USA

3 University of California – Los Angeles, Los Angeles, CA 90095, USA

4 Pennsylvania State University, University Park, PA, USA

5 University of Arizona, Tucson, AZ, USA

6 Earth System Science Interdisciplinary Center, University of Maryland, College Park, MD, USA

7 CNRM, Université de Toulouse, Météo-France, CNRS, Toulouse, France

8 European Centre for Medium-Range Weather Forecasts, Reading, UK

9 Institute of Tibetan Plateau Research, Chinese Academy of Sciences (CAS), Beijing, China

10 Lawrence Livermore National Laboratory, Livermore, CA, USA

11 Hokkaido University, Sapporo, Japan

12 Korea Institute of Atmospheric Prediction Systems, Seoul, South Korea

13 Indian Institute of Tropical Meteorology, Pune, India

14 Beijing Normal University, Beijing, China

15 Barcelona Supercomputing Centre, Barcelona, Spain

16 Institute of Atmospheric Physics, CAS, Beijing, China

17 Pacific Northwest National Laboratory, Richland, WA 99352, USA

18 National Institute for Space Research (INPE), São José dos Campos, Brazil

19 Climate Simulation and Prediction, Fondazione Centro Euro-Mediterraneo sui Cambiamenti Climatici, Bologna, Italy

20 Meteorological Research Institute, Japan Meteorological Agency, Tsukuba, Japan

21 National Center for Environmental Prediction, College Park, MD, USA

22 Center for Earth System Modeling and Prediction, CMA, Beijing, China

23 Bureau of Meteorology, Melbourne, Australia

24 LASG, Institute of Atmospheric Physics, CAS, Beijing, China

25 NOAA/ESRL and University of Colorado/CIRES, Boulder, CO, USA

26 Tsinghua University, Beijing, China